Universitat de Barcelona

Facultat de Física

Master in Astrophysics, Particle Physics and Cosmology

Unitarisation of WW Scattering and Interpretation of a 2 TeV Resonance in a Strongly Interacting Electroweak Symmetry-Breaking Sector

Final project 2014/15:
Pere Arnan

Advisor: Domènec Espriu

Abstract

In this work we introduce and combine an effective Lagrangian formalism with the inverse amplitude method to unitarize $W_LW_L \to W_LW_L$ and $Z_LZ_L \to Z_LZ_L$ amplitudes in an extended electroweak symmetry breaking sector. We derive the unitarisation method via dispersion relations, and discuss different ways of finding the possible resonant states. We compare the two amplitudes calculated with the equivalence theorem approximation and with an exact computation. Moreover, since a diboson excess has been observed near 2 TeV —albeit with very limited statistical significance— in WW, WZ and ZZ final states at the LHC experiments, we constrain the Lagrangian low-energy parameters by limiting the region of the parameter space where a resonance around 2 TeV may appear, and also derive the width of these resonances. Computing the cross-section for two processes we get an idea of how the signal varies along the parameter space, and from the amplitudes we introduce unitarized form factors and vertex functions to allow for a proper treatment of the resonances in Monte Carlo generators and a more precise comparison with experiment.

Contents

1 Introduction

In 2012, ATLAS [1] and CMS [2] discovered a scalar that behave as the Higgs boson, and poured some light in the possible pattern of electroweak (EW) symmetry breaking. The mass of the found scalar particle is about 125 GeV and it is a firm candidate to be considered as the Higgs and to complete the Minimal Standard Model (MSM). However, the dynamical origin of the Higgs and hence of the electroweak symmetry breaking sector (EWSBS) is yet to be elucidated, suggesting existence of a theory beyond the Standard Model (SM) to be explored at the LHC Run II.

There has been plenty of works [3–5] trying to reproduce the electroweak symmetry breaking pattern even with an absence of a light scalar by demanding the existence of a new level of compositeness in the electroweak (EW) sector, making the EW theory an effective theory. In most of these papers, the beyond-SM theories are strongly interacting and thus non-perturbative at a certain scale, producing heavier resonant states, which have arisen as the main phenomenological prediction of such theories nowadays, as they are helpful to constrain the Lagrangian couplings.

Since this theories are strongly interacting, they have been clearly inspired by QCD, specially pion physics, whose aim was to reproduce some resonant behaviour within the regime of an effective theory that later could be explained with the fundamental one with quarks and gluons.

The general procedure to find resonances in this kind of effective theories is to focus on gauge boson WW or ZZ scattering in the EW theory and in pion-pion scattering in QCD. One uses the so called chiral perturbation theory (ChPT) [6] that consists in writing an effective Lagrangian only constrained by the symmetry of the theory, allowing to perform a perturbative expansion of the momentum, and particularly in the EW sector it has to reproduce the low energy EW observed behaviour.

This expansion does not violate unitarity appreciably at sufficiently low energies, but at high energies unitarity is not guaranteed. In order to solve this obstacle, one has to unitarise by hand the amplitudes, trying to respect the symmetries and the analytic properties of the amplitudes. In this work we will use the so called inverse amplitude method (IAM), that is derived from dispersion relations.

In June 2015, ATLAS [7] and CMS [8] reported a diboson excess around 2 TeV using the accumulated 8 TeV data, that can be interpreted as one of these resonances mentioned above. ATLAS looks for the invariant mass distribution of a pair of jets that are compatible with a highly boosted W or Z boson and they reported a little excess with a global significance of 2.5σ. CMS combines dijet and final states with one or two leptons and concludes that there is a small excess around 1.8 TeV with 1.8σ.

The aim of this work is to present a non-linear sigma model effective Lagrangian to describe a strongly interacting EWSBS [3], and constrain some of its parameters to the new data reported by ATLAS experiment through the scattering of the longitudinal components of gauge bosons W_L. Many letters concerning this issue have been published since the discovery of the Higgs boson [9–13], computing W_LW_L scattering using the equivalence theorem (ET) approximation or computing them exactly[1] by means of the IAM. Our analysis is presented by first describing the Lagrangian used in our computations, as well as the role of the parameters appearing in it. We discuss a partial wave analysis since we develop an isospin formalism due to the custodial symmetry of our Lagrangian ($SU(2)_L \times SU(2)_R \to SU(2)_V$). We also introduce the IAM deriving it form

[1] By "exactly" we mean that the ET is only applied at certain diagrams at 1 loop level

dispersion relations, and once the amplitudes are unitarised we explain how to find the poles that lead to resonances. In consideration of dealing with the ET approximation, we carry out a comparison between the exact and the ET amplitudes for different values of the Lagrangian parameters, and analyse the advantages and disadvantages of the two methods. Finally we focus on the ATLAS reported excess to interpret this resonances as a iso-scalar or iso-vector[2] state from W_LW_L scattering with the exact amplitudes in the custodial limit[3] and a Higgs of 125 GeV, and we try to constrain some of the effective couplings provided by the effective theory. In pursuance of explaining the signal we compute the cross section of the amplitudes $W^+W^- \to W^+W^-$ and $ZZ \to ZZ$, as a naive way to compare the different values. In an attempt to be able to compare with more conviction the computations with the experiment, we derive the form factor and the vertex function, to be probed in a Monte-Carlo simulation.

2 Electroweak Chiral Lagrangian

The effective Lagrangian containing the electroweak light degrees of freedom that we will consider is inspired by the Non-Linear sigma model

$$\begin{aligned}\mathcal{L} &= -\frac{1}{2}\mathrm{Tr}W_{\mu\nu}W^{\mu\nu} - \frac{1}{4}\mathrm{Tr}B_{\mu\nu}B^{\mu\nu} + \frac{1}{2}\partial_\mu h\partial^\mu h - \frac{M_H^2}{2}h^2 - d_3(\lambda v)h^3 - d_4\frac{\lambda}{4}h^4 \\ &\quad + \frac{v^2}{4}\left(1 + 2a\left(\frac{h}{v}\right) + b\left(\frac{h}{v}\right)^2 + ...\right)\mathrm{Tr}\, D_\mu U^\dagger D^\mu U + \sum a_i\mathcal{O}_i\,.\end{aligned} \tag{1}$$

where

$$U = \exp\left(i\,\frac{w\cdot\tau}{v}\right) \quad \text{and,} \quad D_\mu U = \partial_\mu U + \frac{1}{2}igW_\mu^i\tau^i U - \frac{1}{2}ig'B_\mu^i U\tau^3. \tag{2}$$

The w are the three Goldstone of the global group $SU(2)_L \times SU(2)_R \to SU(2)_V$. This symmetry breaking is the minimal pattern to provide the longitudinal components to the $W^\pm$ and Z and emerging from phenomenology. The Higgs field h is a gauge and $SU(2)_L \times SU(2)_R$ singlet and the $\mathcal{O}_i$ are a set of higher dimensional operators. In an energy expansion and at the next-to-leading order it is sufficient to consider the $O(p^4)$ operators. This formulation is strictly equivalent to others where the Higgs is introduced as part of a complex doublet, as S-matrix elements are independent of the parameterization.

The operators $\mathcal{O}_i$ include the complete set of operators defined e.g. in [3; 9; 16]. As previously stated, we will be interested in WW scattering and work in the strict custodial limit. Therefore, only a restrict number of operators have to be considered; namely of the possible 13 $O(p^4)$ operators only two O_4 and O_5 will contribute to W_LW_L scattering[4] in the custodial limit:

$$\mathcal{O}_4 = \mathrm{Tr}\left[V_\mu V_\nu\right]\mathrm{Tr}\left[V^\mu V^\nu\right] \qquad \mathcal{O}_5 = \mathrm{Tr}\left[V_\mu V^\mu\right]\mathrm{Tr}\left[V_\nu V^\nu\right], \tag{3}$$

where $V_\mu = (D_\mu U)\,U^\dagger$. We could easily extend the analysis to include non-custodial contributions, but we see little or no reason to do so at present.

[2]Notice that if there is signal in the three channels, the resonance should not be iso-scalar, but as pointed in [14] the huge background makes the signal difficult to interpret

[3]In the non-custodial limit iso-tensor states may appear as physical states as in [15]

[4]When we talk about WW or W_LW_L scattering we refer generically to any scattering of vector bosons. Concrete processes are specified when needed.

The parameters a and b control the coupling of the Higgs to the gauge sector [5]. Couplings containing higher powers of h/v do not enter WW scattering and they have not been included in (1). The two additional parameters d_3, and d_4 parameterize the three- and four-point interactions of the Higgs field. The MSM case corresponds to setting $a = b = d_3 = d_4 = 1$ in Eq. (1). Current LHC results give the following bounds for a, $a_{4,5}$:

$$a = [0.67, 1.33], \qquad a_4 = [-0.094, 0.10], \qquad a_5 = [-0.23, 0.26] \qquad 90\%\text{CL} \tag{4}$$

see [17; 18] . Present data clearly favours values of a close to the MSM value ($a = 1$). We shall consider here this case and the $a = 0.95$ one, in order to see whether there is much different phenomenology when getting a little apart of the MSM. $a > 1$ will not be considered since a previous work [11] shows that it has a quite different behaviour and many problems arise. The parameter b is almost totally undetermined at present and actually does not play a very relevant role in the present discussion. We will assume $b = a^2$ because then there is no inelastic contribution $WW \to hh$ in the scalar channel and simplifies the computations substantially. Some works involving inelastic channels can be found in [5; 12; 13].

We also have to bear in mind that effective theories have a cut-off. In this case, our cut-off is set to $\Lambda = 4\pi v \approx 3$ TeV, where v is the Higgs v.e.v.

3 Partial Wave Analysis

As long as we assume exact custodial symmetry, we are able to develop an isospin (I) formalism for our amplitudes. Since we are dealing with two particle scattering, our isospin amplitudes are divided in the $I = 0, 1$ or 2 channels. The amplitude $A(W_L^a(p^a) + W_L^b(p^b) \to W^c(p^c)_L + W^d(p^d)_L)$ will be denoted by $A^{abcd}(p^a, p^b, p^c, p^d)$. Using isospin and Bose symmetries this amplitude can be expressed in terms of a universal function as

$$A^{abcd}(p^a, p^b, p^c, p^d) = \delta^{ab}\delta^{cd}A(s,t,u) + \delta^{ac}\delta^{bd}A(t,s,u) + \delta^{ad}\delta^{bc}A(u,t,s). \tag{5}$$

with $A(s,t,u) = A^{+-00}(p^+, p^-, p^0, p'^0)$. The fixed-isospin amplitudes are given by the following combinations

$$\begin{aligned} T_0(s,t,u) &= 3A(s,t,u) + A(t,s,u) + A(u,t,s) \\ T_1(s,t,u) &= A(t,s,u) - A(u,t,s) \\ T_2(s,t,u) &= A(t,s,u) + A(u,t,s)\,. \end{aligned} \tag{6}$$

In writing these expressions we assume exact crossing symmetry [5]. We also write the reciprocal relations (also assuming exact crossing symmetry)

$$\begin{aligned} A^{+0+0}(s,t,u) &= \frac{1}{2}T_1(s,t,u) + \frac{1}{2}T_2(s,t,u) \\ A^{+-+-}(s,t,u) &= \frac{1}{3}T_0(s,t,u) + \frac{1}{2}T_1(s,t,u) + \frac{1}{6}T_2(s,t,u) \\ A^{++++}(s,t,u) &= T_2(s,t,u) \\ A^{0000}(s,t,u) &= \frac{1}{3}T_0(s,t,u) + \frac{2}{3}T_2(s,t,u)\,. \end{aligned} \tag{7}$$

[5] This remark is pertinent because amplitudes involving longitudinally polarized bosons are not crossing symmetric. The formulae can be easily extended to this case but become somewhat more involved and will not be reported here. See [9].

Other amplitudes (such as e.g. $A^{+-00}(s,t,u)$) can be obtained trivially from the previous ones using obvious symmetries (and crossing symmetry too).

The partial wave amplitudes for fixed isospin I and total angular momentum J are defined by

$$t_{IJ}(s) = \frac{1}{64\pi}\int_{-1}^{1} d(\cos\theta) P_J(\cos\theta) T_I(s,t,u)\,, \tag{8}$$

where the $P_J(x)$ are the Legendre polynomials and $t = (1-\cos\theta)(4M_W^2 - s)/2$, $u = (1+\cos\theta)(4M_W^2 - s)/2$ with M_W being the W, Z mass t_{00}, t_{11} and t_{20} are the first non-vanishing partial waves in the present case. Working with partial waves is useful because their unitarity properties are easier to check and implement. This unitarity requires that [19]

$$\begin{aligned} |t_{IJ}| &< 1\,, \\ \mathrm{Im}t_{IJ} &= \sigma(s)|t_{IJ}|^2 \end{aligned} \tag{9}$$

where $\sigma(s) = \sqrt{1 - 4M_W^2/s}$ is the two-body phase space. Once obtained the partial waves, ChPT allows us to perform an expansion on the external momentum such as

$$t_{IJ} = t_{IJ}^{(0)} + t_{IJ}^{(1)} + ... \tag{10}$$

In our case, this expansion violates unitarity. This is where we use the IAM we explain below to unitarise them, i.e, to fulfil Equation (9).

4 The Inverse Amplitude Method

As we just mentioned, Equation (10) might violate unitarity at sufficiently high energies. In fact, the terms in the perturbation only respect unitarity perturbatively, namely

$$\begin{aligned} \mathrm{Im}t_{IJ}^{(0)} &= 0 \\ \mathrm{Im}t_{IJ}^{(1)} &= \sigma {t_{IJ}^{(0)}}^2\,. \end{aligned} \tag{11}$$

We need a method to unitarise these amplitudes and at the same time keep the proper analytic properties of the partial waves. We will derive the IAM and make use of it for our following calculations.

4.1 Derivation of the IAM at 1 loop

From S-matrix theory we know that the partial waves should present a characteristic analytic structure in the complex s plane. For WW scattering processes, they are analytic except for a right cut (unitary cut) for $4M_W^2 < s < \infty$ and a left cut for $-\infty < s < 0$, the last cut is needed in order to obey crossing symmetry. Knowing the analytic structure of the partial waves, we can construct an integral equation known as dispersion relation by applying Cauchy's theorem to our amplitudes

$$t_{IJ} = C_0 + C_1 s + C_2 s^2 + \frac{s^3}{\pi}\int_{4M^2}^{\infty} \frac{\mathrm{Im}t_{IJ}(s')}{s'^3(s'-s-i\epsilon)} ds' + \frac{s^3}{\pi}\int_{-\infty}^{0} \frac{\mathrm{Im}t_{IJ}(s')}{s'^3(s'-s-i\epsilon)} ds'\,. \tag{12}$$

This is called a thrice-subtracted dispersion relation, where the last two terms represent the left and right cuts. The reason to expand up to order s^3 (three subtractions) is because we need the integral contour to vanish at

infinity, and since our amplitudes contain $O(p^4)$ terms that behave as s^2 at high energies, we need s^3 terms or higher in the denominator in order to cancel the contour integral. The same reasoning would be implemented if we were dealing with higher order operators and we would need more subtractions to the dispersion relation, but at one loop it is sufficient to deal with three subtractions.

With the help of the ChPT expansion in (10), we can easily put Equation 12 as a function of the perturbative partial waves. By comparison, since we know that $t_{IJ}^{(0)}$ is real and it has the form of

$$t_{IJ}^{(0)} = a_0 + a_1 s \ , \tag{13}$$

and the only imaginary part can come from $t_{IJ}^{(1)}$, that has the proper analytic form

$$t_{IJ}^{(1)} = b_0 + b_1 s + b_2 s^2 + \frac{s^3}{\pi}\int_{4M^2}^{\infty} \frac{\mathrm{Im}t_{IJ}^{(1)}(s')}{s'^3(s'-s-i\epsilon)}ds' + \frac{s^3}{\pi}\int_{-\infty}^{0} \frac{\mathrm{Im}t_{IJ}^{(1)}(s')}{s'^3(s'-s-i\epsilon)}ds' \ , \tag{14}$$

then we are lead to

$$t_{IJ} = a_0 + b_0 + (a_1+b_1)s + b_2 s^2 + \frac{s^3}{\pi}\int_{4M^2}^{\infty} \frac{\mathrm{Im}t_{IJ}^{(1)}(s')}{s'^3(s'-s-i\epsilon)}ds' + \frac{s^3}{\pi}\int_{-\infty}^{0} \frac{\mathrm{Im}t_{IJ}^{(1)}(s')}{s'^3(s'-s-i\epsilon)}ds' \ . \tag{15}$$

This is nothing new, since we have an amplitude that obeys a certain perturbative unitarity relations (11) but not the full one (9). Our next step is to apply this ChPT combined with the full unitarity relation. In order to do that we claim that the function $1/t_{IJ}$ carries the same analytic structure of t_{IJ}. Hence, we define a function as

$$D = \frac{{t_{IJ}^{(0)}}^2}{t_{IJ}} \tag{16}$$

where the numerator plays the role of easing the reasoning. We can construct an analogous dispersion relation for the function D neglecting the possible infinity contributions arising from the zeros of the partial wave:

$$D = D_0 + D_1 s + D_2 s^2 + + \frac{s^3}{\pi}\int_{4M^2}^{\infty} \frac{\mathrm{Im}D(s')}{s'^3(s'-s-i\epsilon)}ds' + \frac{s^3}{\pi}\int_{-\infty}^{0} \frac{\mathrm{Im}D(s')}{s'^3(s'-s-i\epsilon)}ds' \ , \tag{17}$$

imposing unitarity we have

$$\mathrm{Im}D = -{t_{IJ}^{(0)}}^2 \frac{\mathrm{Im}t_{IJ}}{|t_{IJ}|^2} = -{t_{IJ}^{(0)}}^2 \sigma = -\mathrm{Im}t_{IJ}^{(1)} \tag{18}$$

and by performing the same perturbative treatment as before we arrive at

$$D(s) = \frac{{t_{IJ}^{(0)}}^2}{t_{IJ}} = a_0 - b_0 + (a_1 - b_1)s - b_2 s^2 - \frac{s^3}{\pi}\int_{4M^2}^{\infty} \frac{\mathrm{Im}t_{IJ}^{(1)}(s')}{s'^3(s'-s-i\epsilon)}ds' - \frac{s^3}{\pi}\int_{-\infty}^{0} \frac{\mathrm{Im}t_{IJ}^{(1)}(s')}{s'^3(s'-s-i\epsilon)}ds' \ . \tag{19}$$

Notice that the unitary relation only holds exactly on the right cut, so we have done the approximation $\mathrm{Im}D \simeq -\mathrm{Im}t_{IJ}^{(1)}$ for the left cut. From Equation 19 we can identify that

$$t_{IJ} = \frac{{t_{IJ}^{(0)}}^2}{t_{IJ}^{(0)} - t_{IJ}^{(1)}} \ . \tag{20}$$

This last equation is the so called IAM amplitude. It fulfills unitarity relation exactly and has the proper analytic cuts. This form of the partial wave amplitudes is used in different channels to compute resonances and cross sections in what follows of the present work. The poles in the respective unitarised partial wave amplitudes dictate the presence or absence of EWSBS resonances in the different channels. Here we do not derive the inelastic case or the massless one. They are nicely derived in [13]. The IAM has been proven useful before in nuclear physics. It is able to reproduce the poles related to the ρ and the σ mesons in $\pi\pi$ scattering in some of the works in [20], and it has been used in some works on elucidating the nature of the EWSBS [9; 11–13; 20].

4.2 Finding resonance poles

Once applied the IAM to our amplitudes, we should look for a resonance pole in each channel. In order to do that, we display two methods and comment on their strengths and weaknesses respectively. We only interpret the pole as a resonance if this pole lays in the second Riemann sheet (negative imaginary part). If the pole lays in the first Riemann sheet it is considered unphysical, hereby the region embraced by the pole is automatically discarded. The first method is the formal one and consists of performing an analytic continuation of the amplitude provided that the S matrix is a unitary matrix. The second method is an approximation only suitable when the pole is near enough the real axis, and it does not need explicitly the analytic continuation.

- *Method with Analytic Continuation*

  In order to perform a continuation to the second Riemann sheet, we could simply tune the logarithms of our amplitudes such as

  $$\log^{II}(-z) = \log|z| + i(\arg z - \pi)\ , \tag{21}$$

  or in a more formal attempt to have an analytic expression for the second sheet, we use the unitarity property of the S matrix:

  $$S^{II} = \frac{1}{S^I}, \tag{22}$$

  where the super-index refer to the first (physical) and second (unphyisical) Riemann sheets. This equation implies that the continuation of a partial wave amplitude from the first sheet to the second one is [13; 21]

  $$t^{II}_{IJ} = \frac{t^I_{IJ}}{1 - 2i\sigma t^I_{IJ}}\ . \tag{23}$$

  Therefore we can find the pole on the second Riemann sheet by looking for the following zero in the massless case:

  $$t^I_{IJ}(s) + i/2 = 0 \tag{24}$$

  or what is the same for the IAM amplitude at 1-loop,

  $$t^{(0)}_{IJ}(s) - t^{(1)}_{IJ}(s) - 2i[t^{(1)}_{IJ}(s)]^2 = 0\ , \tag{25}$$

  and we locate the complex pole $s = (m - i\Gamma/2)^2$ directly. In Figure 1 we depict the three different channels in a region of the parameter space a_4, a_5 where there is a pole in the second Riemann sheet for the vector and the scalar channels, while the tensor channel presents no resonances. This method is exact, but it is computationally harder than the one we present next.

- *Method for Poles Near the Real Axis*

  This method is very easy to implement and it has a nice result when comparing to the exact one. The first step is to look for the zero of the real part of the denominator of the IAM amplitude, namely:

  $$\mathrm{Re}(t^{(0)}_{IJ}(s) - t^{(1)}_{IJ}(s)) \equiv \mathrm{ReDen}(s) = 0\ . \tag{26}$$

  At this point we obtain what we consider the real part of the pole ($s = m^2$). Making a Taylor expansion of the denominator around m^2 up to order one

  $$\begin{aligned} \mathrm{Den}(s) &= \mathrm{Den}(m^2) + \frac{d\mathrm{Den}}{ds}\Big|_{m^2}(s - m^2) + ... \\ &= \frac{d\mathrm{Den}}{ds}\Big|_{m^2}(s - m^2) + ... \end{aligned} \tag{27}$$

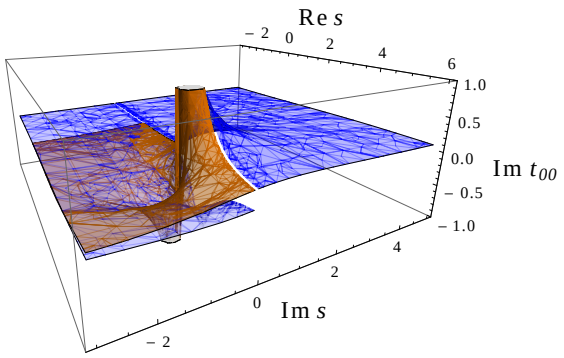

(a) Scalar

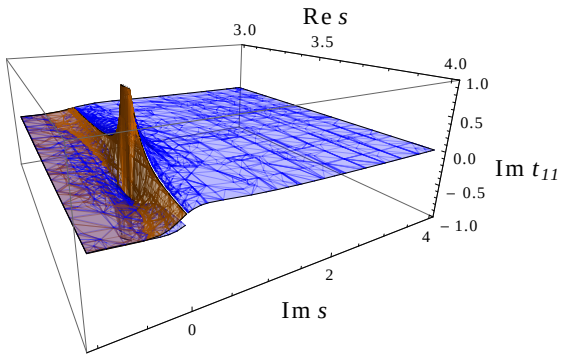

(b) Vector

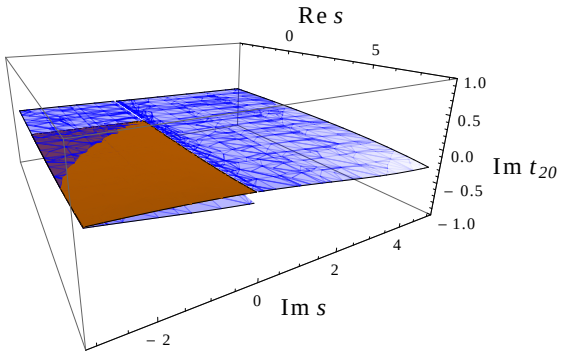

(c) Tensor

Figure 1: For $a = 1$,$b = 1$ and $a_4 = 0.0002$, $a_5 = -0.0001$, we plot the first Riemann sheet (blue) and the second one (brown) for the imaginary part of the amplitude in the three different channels. (a) The scalar amplitude has a pole on the second Riemann sheet corresponding to $M = 2064$ GeV. (b) The vector amplitude has a pole on the second Riemann sheet corresponding to $M = 1881$ GeV. Notice the different range compared with the scalar channel as the resonance is narrower in this channel. (c) The tensor channel does not present a resonant behaviour. In this channel and for this values of a and b the resonances, if present, only appear on the first Riemann sheet.

we perform a "continuation" putting $s_{\rm pole} = (m - i\Gamma/2)^2$ in Equation 27, and take the imaginary part of the denominator, approximating $\mathrm{ImDen}(s_{\rm pole}) \simeq \mathrm{ImDen}(m^2)$. All in all we end up with

$$\mathrm{ImDen}(m^2) = -\frac{d\mathrm{Den}}{ds}\Big|_{m^2} m\Gamma \,, \tag{28}$$

and from here we can extract Γ. The positive thing of this method is that we do not search directly for complex roots. Instead, we find a real root of a real function and then we find the complex part of that pole. Finding the poles in this way is only valid when they are near the real axis.

Setting $a = 1$ and $b = a^2$ for different values of a_4, a_5, the maximum numerical difference between the two methods is found in the resonances of the scalar channel where the difference is in the second digit. Curiously,

the minimum difference is also found in the scalar channel, being the mass and the width equal up to the 6th digit. We will generally use the second method, which is easier to implement.

5 Goodness of the Equivalence Theorem

Once included the electroweak interactions, the Goldstone bosons "disappear" and become the longitudinal components of the gauge bosons. Somehow we can identify the Goldsone bosons and their behaviour with that of the gauge bosons. This is a simple explained version of the ET, and a deeper look can be found in [22; 23]. Expressing mathematically the theorem is very simple

$$T(W_L W_L \to W_L W_L) \simeq T(\omega\omega \to \omega\omega) + \mathcal{O}\left(\frac{M_W}{\sqrt{s}}\right), \tag{29}$$

where M_W is the mass of the gauge boson and $\sqrt{s}$ is the center of mass energy. Looking at the equation, one realizes that ET allows us to identify the longitudinal components of the gauge bosons with the Goldstone bosons at energies $\sqrt{s} \gg M_W$. This approximation makes the calculation of the amplitudes much easier, since now we treat scalar particles. Therefore the couplings of the Goldstone bosons with the gauge bosons vanish ($g = g' = 0$), and the only degrees of freedom left will be the GB (massless in the Landau gauge [24]), and the Higgs boson.

In this section our aim is to test the use of the ET in front of the exact amplitudes at 1-loop. ET amplitudes have been calculated in [25] while the exact amplitudes can be found in [9; 11]. The main obstacle of this approximation is that with the MSM values for the parameters a and b ($a = b = 1$), it is not able to produce dynamical resonances in the parameter space a_4, a_5 with the IAM method, as the tree level amplitude vanishes when $a = 1$. For that reason, all of our computations are done with $a = 0.95$ and $b = a^2$.

In order to make a first comparison, we plot in Figure 2 the chiral expansion for the three isospin channels together with the same amplitudes obtained with the IAM[6]. We placed ourselves in a region of the parameter space yielding a vector and a scalar resonances both with the ET approximation and the exact calculation. We see that being the chiral expansion plots very similar, the IAM plots differ quite significantly. The scalar resonance is $M_S^{\text{exact}} \simeq 2400$ GeV and $M_S^{\text{ET}} \simeq 1700$ GeV, while the vector resonance reads $M_V^{\text{exact}} \simeq 2200$ GeV and $M_V^{\text{ET}} \simeq 1700$ GeV. The difference is notable and it is also very appreciable in the figure. Furthermore, we can see that the widths are much broader for the exact amplitudes, but that comparison is delicate because we are testing different masses.

In pursuance of comparing the relation mass-width, we show in Figure 3 the relation between the mass and the width for different poles found in a sweep of the parameter space a_4, a_5 for the three channels. for the same number of points, we may appreciate that the exact amplitude has more dispersion than the ET amplitude. The resonance poles in the ET case have lower masses in general, and we see that for a fixed mass the absolute value of Γ is also lower using the ET.

Seeming that the results with the ET are substantially different from the exact ones, we claim that for the purpose of sweeping the $a_4 - a_5$ plane looking for resonances it is a great approximation as we see in Figure 4. The presence of resonances in the parameter space is practically the same[7]: the ET allows a little bit more

[6] In this plots we work in TeV since the amplitudes computed the equivalence theorem work in the TeV scale

[7] One can find such comparisons for $a = 1.3$ in [11] for the exact computations and in [26] with the ET approximation.

space without resonances near $a_4 = a_5 = 0$. Although the picture is almost the same, the value of the masses and the widths is remarkably different, as stated before.

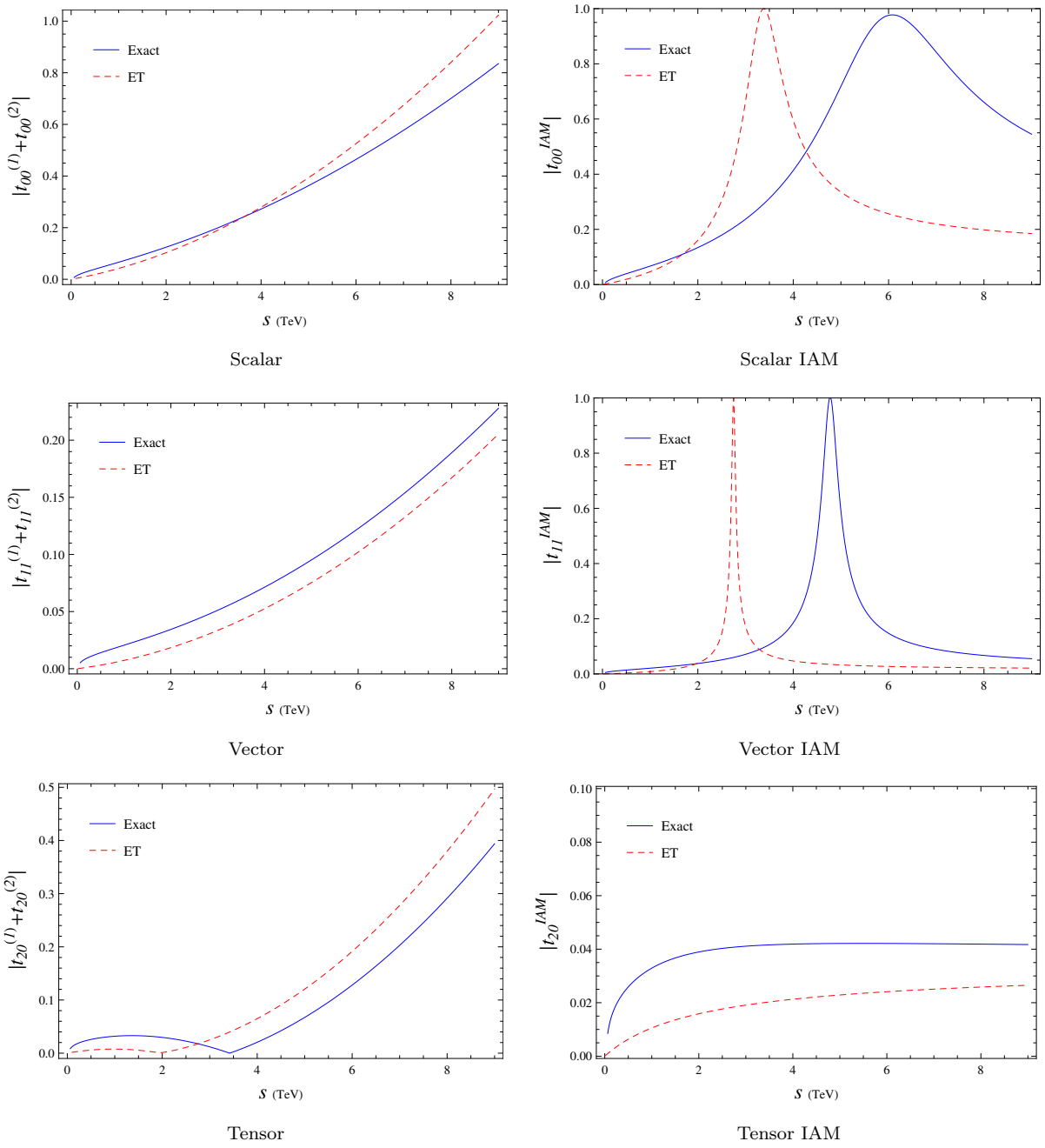

Figure 2: For $a = 0.95$,$b = a^2$ and $a_4 = 0.000325$, $a_5 = -0.000105$, we plot the perturbative chiral expansion and the IAM amplitudes for the three channels. The scalar channel yields a resonance at $M_S^{\text{exact}} \simeq 2400$ GeV, $M_S^{\text{ET}} \simeq 1700$ GeV. The vector channel at $M_V^{\text{exact}} \simeq 2200$ GeV, $M_V^{\text{ET}} \simeq 1700$ GeV. The tensor channel does not contain any resonance. Notice the different range of the $y-$axis in the plots. The ET amplitudes used are computed in [25] and the exact ones in [9; 11], as in Figures 3 and 4.

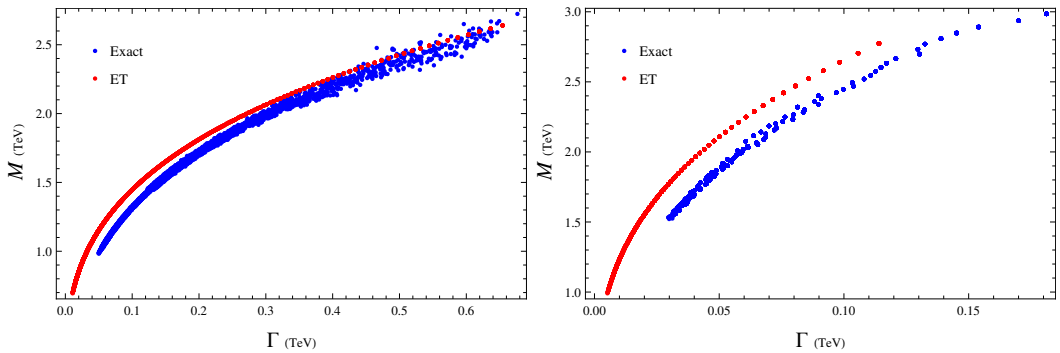

(a) Scalar

(b) Vector

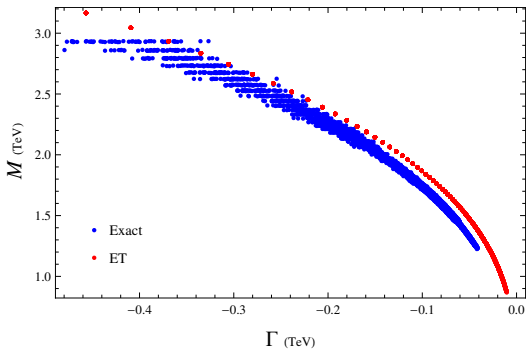

(c) Tensor

Figure 3: For $a = 0.95$,$b = a^2$, we display 4000 points corresponding to resonance poles, comparing the ET and the exact resonances plotting mass vs width for the three different channels. Notice the dispersion of the exact calculation while in the ET approximation the trend is quite clear.

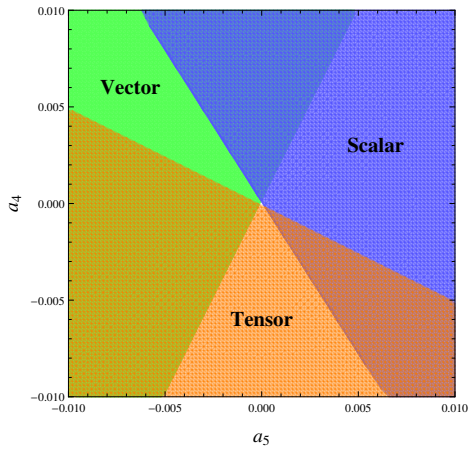

(a) ET

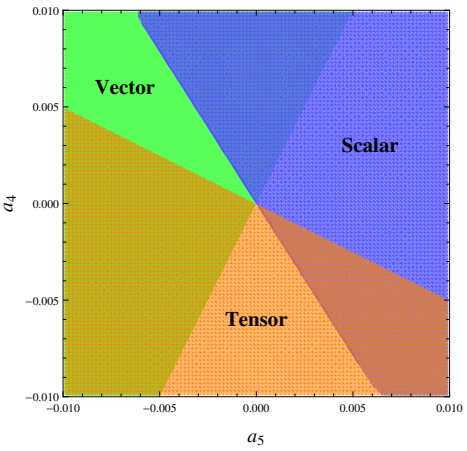

(b) Exact

Figure 4: For $a = 0.95$,$b = a^2$, the plot shows a sweep of the $a_4 - a_5$ plane where a resonance is found in the ET approximation or in the exact calculation. Those resonances are classified in the three different channels. Notice that there are several regions of overlapping, and the region $a_4 = a_5 = 0$ has no poles.

6 Constraining the effective Lagrangian coefficients

The data collected by ATLAS and CMS experimentalists fits with a 2 TeV resonance in diboson experiments. In this section we should analyse and constrain the regions in the parameter space where this may occur in our model for $a = 1$ and $a = 0.95$. For that reason, we perform the computations using the exact amplitudes found in [9; 10] and look for resonances with $1.8 < M < 2.2$ TeV.

6.1 $a = 1$

After requiring a resonance in the vector channel with a mass in the quoted range one gets in a $a_4 - a_5$ plane the region shown on the left in Figure 5 for $a = 1$. An analogous procedure but assuming that the resonance is the $I = 0, J = 0$ channel results in the allowed region in the $a_4 - a_5$ plane depicted in Figure 6.

We would like to emphasize the very limited range of variation for the parameters that is shown in Figures 5 and 6. The constants a_4 and a_5 lay in the small region $|a_4|, |a_5| < 5 \times 10^{-4}$. (This region includes of course the MSM value $a_4 = a_5 = 0$ but —obviously— there are no resonances there.)

In order to convey a picture of the sort of predictive power of unitarisation techniques we plot in Figure 7 the allowed bands in the broader range $|a_4|, |a_5| < 0.01$ that was considered in a previous work [9] as still being phenomenologically acceptable. Indeed, setting even a relatively loose bound for the mass of the resonance restricts the range of variation of the relevant low-energy constants enormously. In the same figure we show a blown-up of the region where *both* a scalar and a vector resonance in this mass range may coexist. The dashed area is excluded as acceptable for effective EWSBS theories (see [11]). In Figure 8 we show the compatible vector or scalar resonances assuming that the 2 TeV resonance is scalar or vectorial.

We may notice that the width of the scalar channel is in general larger than in the vector channel. This fact is in agreement with Figure 2, when we were testing the ET.

6.2 $a = 0.95$

For $a = 0.95$, we show in Figure 9 the same picture as in Figure 5. Analogously, in Figure 10 we show the region of the parameter space where a scalar resonance mass between 1.8 and 2.2 TeV is found. We see that there is a wider region of the parameter space where both vector and scalar masses are suitable to the range of masses demanded. Nonetheless, the restriction of the parameter space due to this demand is very similar to the one taking $a = 1$. The main difference with the $a = 1$ plots, is that the width increases significantly in both channels, but specially in the scalar one. In the scalar channel, the width is multiplied by a factor of 4, while in the vector channel it is increased by a factor from 2 to 4. This trend may suggest that the lower the a parameter, the wider is the resonance, and it gives us some intuition in order to compare with the experiment in future works.

We could also present the same plots as in the $a = 1$ case corresponding to Figures 7 and 8, but these new plots would not change the argument made previously as they are very similar. Therefore we do not show them.

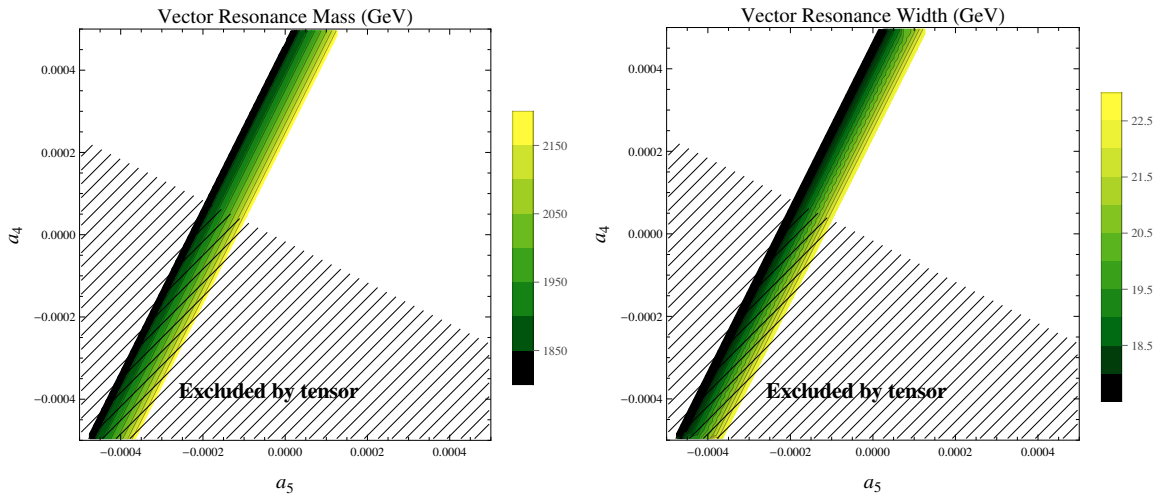

(a) (b)

Figure 5: For $a = 1$ and $b = 1$: (a) allowed values for a_4, a_5 corresponding to a vector resonance with a mass between 1.8 TeV and 2.2 TeV. Note the extremely limited range of variation that is allowed in the figure for the low-energy constants. (b) The corresponding widths as predicted by unitarity using the IAM method. The characteristic value is 20 GeV, quite narrow for such a large mass. The dashed area is excluded on causality grounds stemming from the $I = 2$ channel.

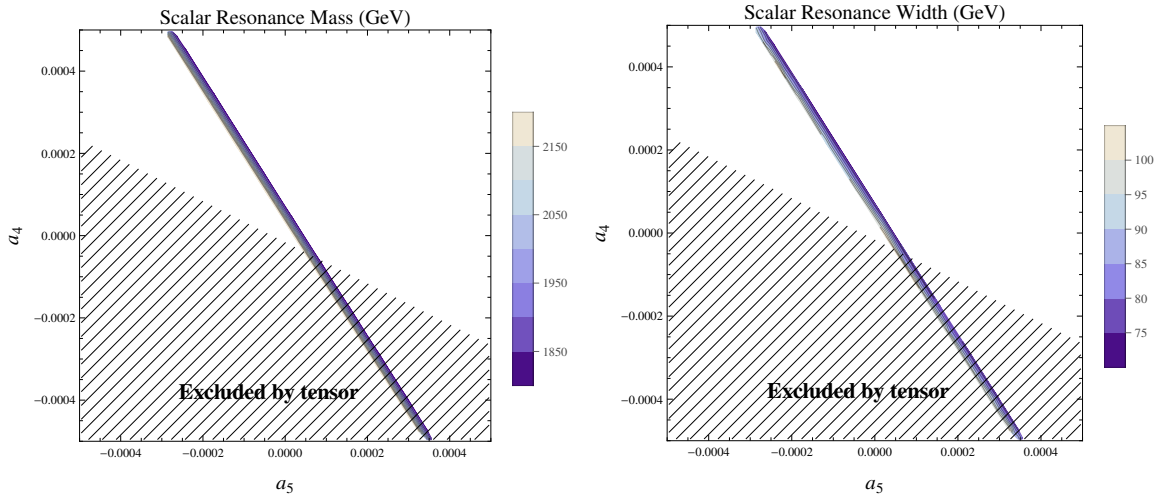

(a) (b)

Figure 6: For $a = 1$ and $b = 1$: (a) allowed values for a_4, a_5 corresponding to a scalar resonance with a mass between 1.8 TeV and 2.2 TeV. (b) The corresponding widths as predicted by unitarity using the IAM method; characteristic values are in the 70-100 GeV range.

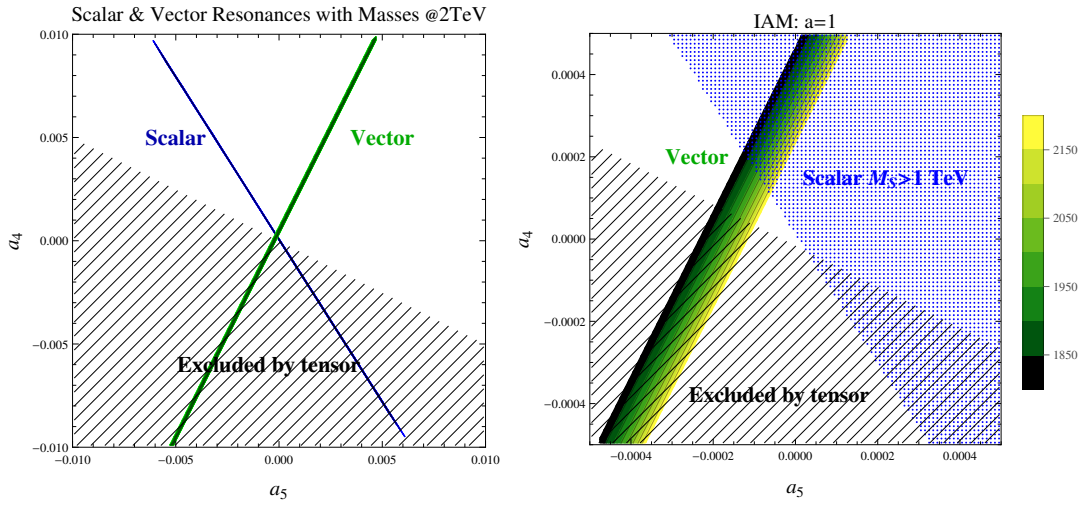

(a) (b)

Figure 7: (a) This plot makes visible how restrictive for the low-energy constants of the EWSBS effective Lagrangian becomes the requirement of yielding a resonance in the 1.8 TeV $< M <$ 2.2 TeV range. The dashed area is excluded on causality grounds. (b) Blow-up of the region of overlap where vector and scalar resonances may coexist. The broad strip shows the region of admissible vector resonances with masses in the 1.8-2.2 TeV range. The shaded area in the upper-right part contains scalar resonances of mass > 1 TeV. For $a = 0.95$ this picture is very similar and we think that to get the idea it is sufficient with this one.

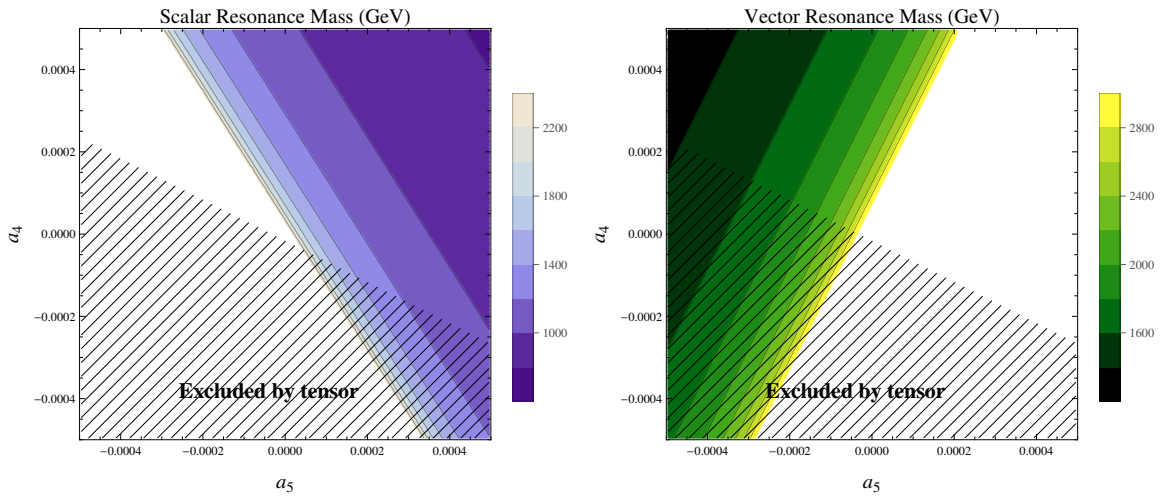

(a) (b)

Figure 8: (a) Viable scalar resonance masses in the region of interest in the a_4-a_5 plane for $a = 1$ assuming a vector resonance in the 1.8 TeV $< M <$ 2.2 TeV range. (b) The reverse situation: assuming a scalar mass in the 1.8 TeV $< M <$ 2.2 TeV range and depicting the possible values for a vector resonance compatible with it. For $a = 0.95$ this picture is very similar and we think that to get the idea it is sufficient with this one.

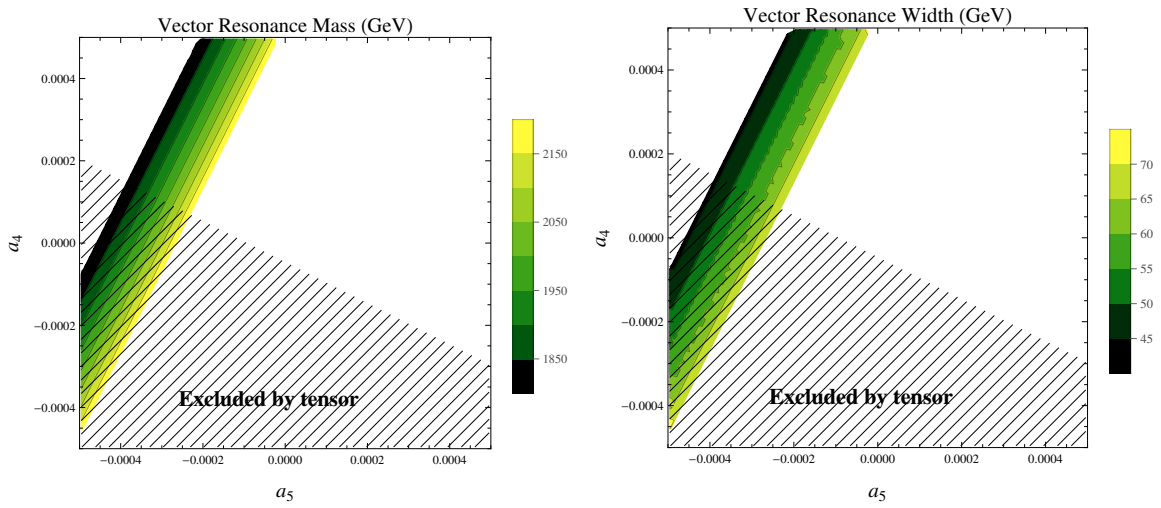

(a) (b)

Figure 9: For $a = 0.95$ and $b = a^2$: (a) allowed values for a_4, a_5 corresponding to a vector resonance with a mass between 1.8 TeV and 2.2 TeV. (b) The corresponding widths as predicted by unitarity using the IAM method; characteristic values are in the 40-70 GeV range.

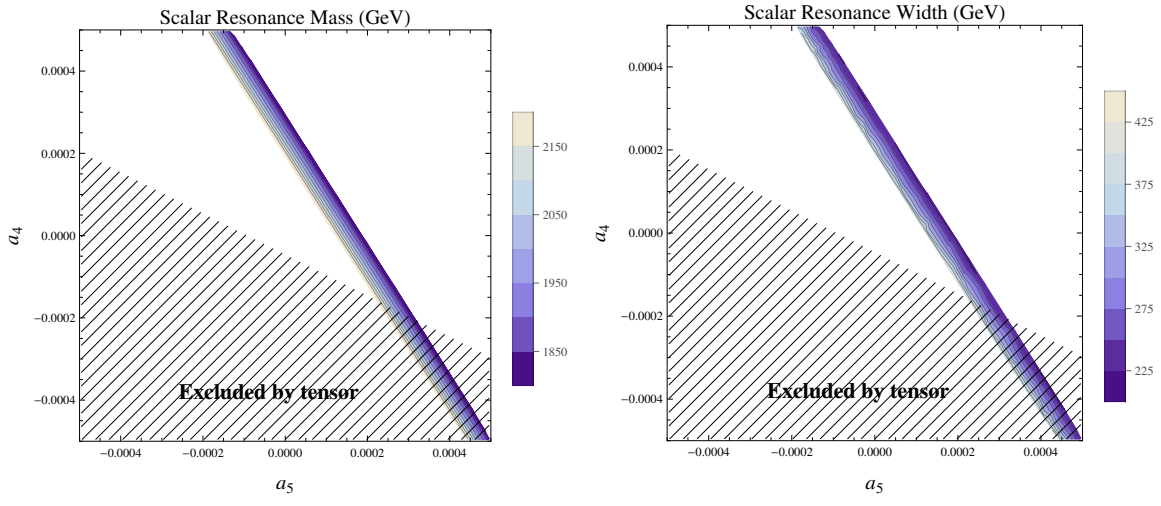

(a) (b)

Figure 10: For $a = 0.95$ and $b = a^2$: (a) allowed values for a_4, a_5 corresponding to a scalar resonance with a mass between 1.8 TeV and 2.2 TeV. (b) The corresponding widths as predicted by unitarity using the IAM method; characteristic values are in the 200-400 GeV range.

7 Experimental visibility of the resonances

The statistics so far available from the LHC experiments is limited. Searching for new particles in the LHC environment is extremely challenging and analysing the contribution of possible resonances to an experimental

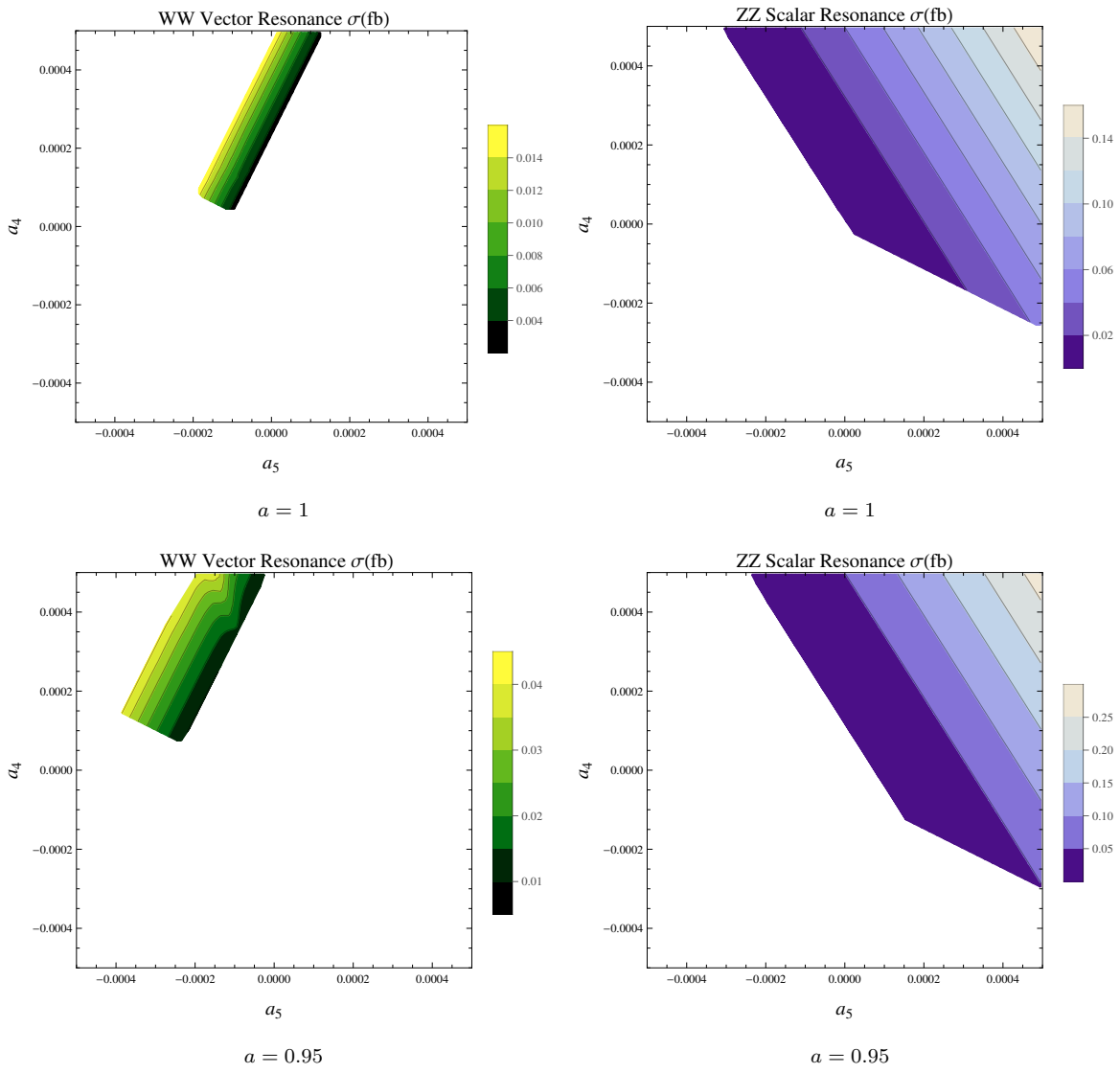

Figure 11: Experimental signal of resonances for $a = 1$ and $a = 0.95$: the resonance cross sections are given in fb, the LHC energy has been taken to be 8 TeV and the EWA approximation is assumed in this calculation. Left: estimated cross section for the process $W_L W_L \to W_L W_L$ as a function of the parameters a_4, a_5 due to a vector resonance. Right: cross section for the process $Z_L Z_L \to Z_L Z_L$ due to a scalar resonance. The contribution from the 125 GeV Higgs is also included in both cases.

signal is not easy without a well defined theoretical model with definite predictions for the couplings, form factors, etc. The IAM method is able not only of predicting resonance masses and widths but also their couplings to the $W_L W_L$. In [9; 11] the experimental signal of the different resonances was compared to that of a MSM Higgs with an identical mass. Because the decay modes are similar (in the vector boson channels that is) and limits on different Higgs masses are very documented, this was a rather intuitive way of presenting the cross-section for possible EWSBS resonances, but it is not that useful for heavy resonances as the signal of an hypothetical Higgs of analogous mass becomes very broad and diluted. This point and several others are

discussed in detail in [9]. Here we shall give very simple estimates of some cross-sections based on the Effective W Approximation (EWA) [27] in a couple of channels. These estimates should be taken as extremely tentative and only relevant to establish comparisons between different masses and channels. In the last section we will introduce form factors and vertex functions to allow for a proper comparison with experiment. Please note that in the amplitudes where scalars contribute the contribution of the 125 GeV Higgs is also included.

Some results for the cross sections are depicted in Figure 11 for $a = 1$ and $a = 0.95$ the processes $W_L^+W_L^- \to W_L^+W_L^-$ and $Z_LZ_L \to Z_LZ_L$. In the first process we quote the contribution from a possible vector $\sim$2 TeV resonance only (a scalar resonance is also possible in this process). In the second case only scalar exchange is possible and its mass is considered as $M_S > 1TeV$. Note that both diboson production modes are sub-dominant at the LHC with respect to gluon production mediated by a top-quark loop and that the possible resonances in the scenario discussed here couple *only* to dibosons.

Compared to the preliminary experimental indications, the results quoted for the cross-sections of these two specific processes are low, particulary for vector resonances, but there are several caveats. First of all, the EWA tends to underestimate the cross-sections and it is difficult to assess its validity in the present kinematical situation. Second, in this region of parameter space the cross-sections do change very quickly with only small changes of the parameters thus adding an element of uncertainty. Finally, the quoted cross sections correspond to considering only the interval $s \in [M - 2\Gamma, M + 2\Gamma]$ so as to have some intuition on the contribution of the resonance itself. It should also be mentioned that, as discussed in [9], there is an enhancement in the $W^+W^- \to W^+W^-$ channel when both the vector and scalar resonances become nearly degenerate; this is possible in a limited region of parameter space. We also see that comparing the two different values of a, the cross section in both processes enhances when we lower a a little bit.

Interesting as partial waves for a given process may be, they are not that useful to implement unitarisation in a Monte Carlo generator in order to make detailed quantitative comparison with experiment. One would need to implement diagrammatic and for that one needs vertex functions and propagators wherewith to construct and compute the contribution from different topologies. Our proposal to tackle this problem is presented next.

8 Introducing form factors

We would like to express any amplitude as the sum of exchanges of resonances in the s, t and u channels, as it is diagrammatically expressed in Figure 12. That is, we decompose, say A^{+0+0}

$$A^{+0+0} = \sum_{IJ}(A_s^{IJ} + A_t^{IJ} + A_u^{IJ}) \tag{30}$$

Not all IJ receive contributions from all three channels. For example, in the case $A^{+0,+0}$ a possible scalar resonance only contributes to the t-channel. In addition, not all processes are resonant in all regions of parameter space, so the above decomposition assumes resonance saturation. Let us now define the vector form factor as[8]

$$\langle W_L^i(p_1)W_L^j(p_2)|J_\mu^k|0\rangle = (p_1 - p_2)_\mu F_V(s)\epsilon^{ijk} \tag{31}$$

[8]conservation of vector current has been used due to $SU(2)$ symmetry.

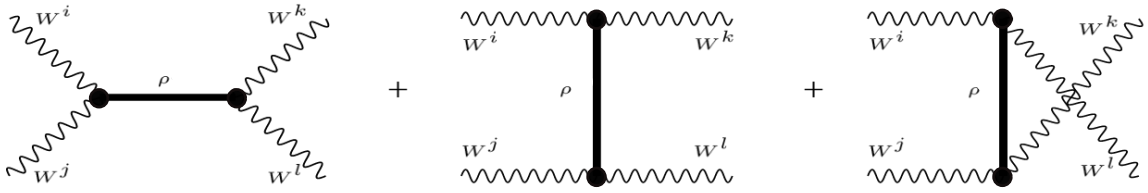

Figure 12: Decomposition of a process in (unitarised) form factors and resonance propagators.

where J_k^μ is the interpolating vector current with isospin index k that creates the resonance ρ and $F_V(s)$ is the vector form factor. From this form factor we derive a vector vertex function K^μ via the relation [28]

$$K^\mu(p_1,p_2) = (p_1-p_2)^\mu F_V(s)(s-M^2_{\rm pole}) \tag{32}$$

Let us focus for instance on the amplitude A^{+0+0} that has potentially contributions from a vector and a tensor. The IAM does exclude the $I=2$ contribution [11] so let us consider A_s^{11} for this process. It can be expressed as

$$A_s^{11} = K^\mu \frac{g_{\mu\nu} - \frac{k_\mu k_\nu}{k^2}}{s-M^2_{\rm pole}} K^{*\nu} = |F_V(s)|^2 (s-M^{*2}_{\rm pole})(-2t-s) = |F_V(s)|^2 (s-M^{*2}_{\rm pole})(-s\cos\theta) \tag{33}$$

where $M_{\rm pole} = M - i\Gamma/2$. Analogous decompositions exist for A_t^{11} and A_u^{11}. In fact we do not need to consider A_t^{11} and A_u^{11} at all because assuming exact isospin symmetry $A^{11}(s,t,u) = (-1)^I A^{11}(s,u,t)$. Here we assume, and it is a necessary ingredient of the present approach, that external lines are on-shell.

On the other hand from unitarisation we know that

$$A^{+0+0} \simeq A^{11} = 96\pi t_{11}(s)\cos\theta, \tag{34}$$

so neglecting further partial waves it is natural to identify

$$|F_V(s)|^2 = -\frac{96\pi t_{11}(s)}{s(s-M^{*2}_{\rm pole})} \tag{35}$$

where for t_{IJ} we use the IAM approximation. Although $|F_V|^2$ should of course be real and positive, when using the identification above we get a tiny imaginary part ($\mathrm{Im}|F_V|^2 \sim 10^{-2}\mathrm{Re}|F_V|^2$) due to the fact that we are missing possible channels (including non-resonant contributions) and terms in the partial wave expansion. However we can regard the description of the amplitude via vertex functions and resonance propagators as quite satisfactory in the regions where resonances are present.

Neglecting the gauge boson mass (quite justified at 2 TeV) unitarity requires the form factor to obey the following relation within a vector dominance region [16]

$$\mathrm{Im}F_V(s) = t_{11}^*(s)F_V(s). \tag{36}$$

Equation (36) allows us to extract the phase of $F_V(s)$. Thus, combining the phase and the modulus we obtain the vector form factor

$$F_V(s) = |F_V(s)| \exp\left(i \arctan \frac{\mathrm{Re}t_{11}}{1-\mathrm{Im}t_{11}} \right). \tag{37}$$

Similar techniques could allow us to define a unitarised scalar form factor $F_S(s)$ and a vertex function directly derived from the unitarised amplitude that in this channel is

$$A^{00} = 32\pi t_{00}(s) \tag{38}$$

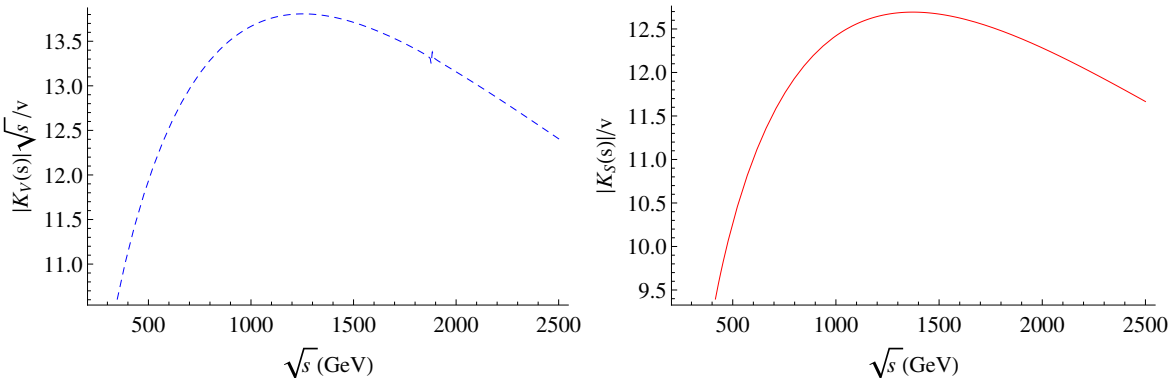

Figure 13: Left: plot of the effective coupling of the vector resonance $K_V(s)\sqrt{s}$ for the value $M = 1881$ GeV corresponding to $a = 1$ $a_4 = 0.0002$,$a_5 = -0.0001$. Right: plot of the effective coupling for a scalar resonance $K_S(s)$ corresponding to the same values of a_4 and a_5 that yields a scalar mass $M = 2064$. Note that in both cases the coupling is quite large, certainly non-perturbative. In fact, on the scalar resonance the effective coupling is ~ 30 times the coupling of a MSM Higgs with identical mass.

and assuming resonance dominance. In Figure 13 we plot the vertex functions $K_V(s)$ and $K_S(s)$ obtained by the method just described:

$$|K_V(s)| \sim |F_V(s)||s - M^2_{\rm pole}|, \qquad |K_S(s)| \sim |F_S(s)||s - M^2_{\rm pole}|. \tag{39}$$

Note that the function $K_V(s)$ is dimensionless while $K_S(s)$ has units of energy. However for vector resonances, the effective coupling is typically $K_V(s)\sqrt{s}$ (see the expression for the form factor and the associated Feynman rule). In the last figure we plot these effective couplings normalised to the scale v. The contribution to the form factor from the 125 GeV Higgs is negligible around the scalar resonance at ~ 2 TeV.

Once we feel confident that the combination of resonant propagators and the vertex functions just given reproduces very satisfactorily the unitarised amplitudes we can pass on this information to Monte Carlo generator practitioners to implement these form factors in a generator.

The expressions for $M_{\rm pole}$, $t_{00}(s)$ and $t_{11}(s)$ needed to reproduce the diagrammatic expansion for the various values of a and a_4, a_5 can be found in [9–11] (and [12; 13] if a full use of the equivalence theorem is made[9]).

9 Conclusions

In this work we explored some phenomenological consequences of a strongly interacting EWSBS. We focused on a non-linear sigma model effective Lagrangian inspired by QCD, and adding the gauge and scalar terms reproducing the EW behaviour at low energies. Introducing some deviations to the MSM via different parameters such as a, b, a_4 or a_5, we were able to perform a partial wave chiral expansion for $W_L W_L$ scattering at 1-loop level using isospin formalism, and in an attempt to restore the unitarity of this expansion we introduced and derived the IAM which unitarises and keeps the analytic properties of the partial waves.

Furthermore, we provided a comparison of the ET with the exact amplitudes, seeing that for the purpose of predicting a resonance mass or width is not the best tool, but in order to reproduce the a_4, a_5 map of scalar,

[9]Please note that t-channel W exchange is not included in some of these works.

vector and tensor poles is a nice approximation at least for $a < 1$, since it cannot reproduce resonant behaviour when the gauge boson-higgs couplings are set to the MSM values.

For this reason we used exact amplitudes to explore the parameter space a_4, a_5 looking for scalar and vector resonances with a mass in the range 1.8 TeV $< M <$ 2.2 TeV —as it would be the case if one considers the preliminary results coming from the LHC experiment to be the first hints of the existence of new $W_L W_L$ interactions— for $a = 1$ and $a = 0.95$, and noticed how the fact of restricting to this mass range constrained the a_4 and a_5 values. We determined the widths of such resonances, which are significantly narrow for $a = 1$ but they do become much broader when $a = 0.95$. We also computed the cross sections for two processes using the EWA for $a = 1$ and $a = 0.95$, one aiming attention at a vector resonance and the other one at a scalar resonance. We saw that when a is lower than one, the signal increases for both processes.

In consideration of performing a deeper analysis on the possible extended EWSBS, we derived the form factor and the vertex function from the amplitudes via a diagrammatic method, paying attention where there is a scalar resonance dominant region or a vector one in the parameter space. We plotted the vertex functions for the scalar and vector channels normalised with the EW scale v and saw that the possible new couplings are larger. These vertex functions and form factors could be included in a full detector simulation, in the interest of comparing directly with experiments.

We hope the second run of LHC to pour some light on the insight of WW scattering, and to confirm or disprove the little excess that appeared in the data of the LHC run I, which has triggered a lot of activity [29]. For future works, it is interesting to focus on $a > 1$ features and the consequences of including inelastic channels like $WW \to hh$ by setting $b \neq a^2$. It is also important to compare different unitarisation methods with the IAM to see if they lead to a similar resonance's behaviour.

Acknowledgements

First of all, I would like to thank my advisor D. Espriu for his great help and even greater patience during the realisation of this work. I want to thank F. Mescia, for his inestimable help with the amplitudes and cross section code.

Besides, I would like to thank my office mates, X.R. Hoffmann, V. Navas and E. Sanmartí for the good moments and helpful — mainly LaTeX— discussions.

I would like to make a special mention to my parents, who supported me without hesitation during the whole career and the master, and bore with my bad mood when things were difficult.

References

[1] G. Aad et al. (ATLAS Collaboration), Phys. Lett. B716, 1 (2012).

[2] S. Chatrchyan et al. (CMS Collaboration), Phys. Lett. B716, 30 (2012).

[3] A. Dobado, D. Espriu and M.J. Herrero, Phys.Lett. B255 (1991) 405; D. Espriu and M.J. Herrero, Nucl.Phys. B373 (1992) 117; M.J. Herrero and E. Ruiz-Morales, Nucl.Phys. B418 (1994) 431; Nucl. Phys.

B 437 (1995) 319; D. Espriu and J. Matias, Phys.Lett. B341 (1995) 332; 1; R. Foadi, M. Jarvinen and F. Sannino, Phys. Rev. D 79, 035010 (2009).

[4] S. Dawson and S. Willenbrock, Phys. Rev. D 40, 2880 (1989); D. A. Dicus and W. W. Repko, Phys. Rev. D 42, 3660 (1990); S. N. Gupta, J. M. Johnson, and W. W. Repko, Phys. Rev. D 48, 2083 (1993); E. Halyo, Mod. Phys. Lett. A 8 (1993) 275; W. D. Goldberger, B. Grinstein and W. Skiba, Phys. Rev. Lett. 100 (2008) 111802

[5] G. F. Giudice, C. Grojean, A. Pomarol and R. Rattazzi, JHEP 0706, 045 (2007); R. Contino, M. Ghezzi, C. Grojean, M. Muhlleitner and M. Spira, JHEP 1307, 035 (2013); R. Alonso, M. B. Gavela, L. Merlo, S. Rigolin and J. Yepes, Phys. Lett. B 722, 330 (2013); R. Alonso, I. Brivio, B. Gavela, L. Merlo and S. Rigolin, JHEP 1412, 034 (2014); G. Buchalla, O. Catà and C. Krause, Nucl. Phys. B 880, 552 (2014); G. Buchalla and O. Cata, JHEP 1207, 101 (2012).

[6] S. Scherer, Adv.Nucl.Phys. **27** (2003) 277

[7] G. Aad et al. (The ATLAS collaboration), arXiv:1506.00962.

[8] V. Khachatryan et al. (The CMS collaboration), JHEP 1408 (2014) 173.

[9] D. Espriu and B. Yencho, Phys. Rev. D 87, no. 5, 055017 (2013).

[10] D. Espriu, F. Mescia and B. Yencho, Phys. Rev. D 88, 055002 (2013).

[11] D. Espriu and F. Mescia, Phys.Rev. D 90, 015035 (2014).

[12] R. Delgado, A. Dobado, and F. Llanes-Estrada, J.Phys. G 41, 025002 (2014); Phys. Rev. Lett. 114, 221803 (2015); D. Barducci, H. Cai, S. De Curtis, F. Llanes-Estrada and S. Moretti, Phys. Rev. D 91, 095013 (2015).

[13] R. Delgado, A. Dobado and F. Llanes-Estrada, Phys.Rev. D 91, 075017 (2015).

[14] B. C. Allanach, B. Gripaios and D. Sutherland, arXiv:1507.01638.

[15] H. Georgi and M. Machacek, Nucl. Phys. B 262, 463 (1985).

[16] A. Dobado, M.J. Herrero, J.R. Peláez and E. Ruiz-Morales, Phys. Rev. D 62 (2000) 0550.

[17] A. Falkowski, F. Riva and A.Urbano, JHEP 1311, 111 (2013).

[18] I. Brivio, T. Corbett, O. J. P. Eboli, M. B. Gavela, J. Gonzalez-Fraile, M. C. Gonzalez-Garcia, L. Merlo and S. Rigolin, JHEP **1403**, 024 (2014).

[19] J. Hamilton and B. Tromborg; *Partial Wave Amplitudes and Resonance Poles*. Oxford University Press (1972)

[20] T.N. Truong, Phys. Rev. Lett. 61 (1988) 2526; A. Dobado, M.J. Herrero and T.N. Truong, Phys.Lett. B235 (1990) 134; A. Dobado and J.R. Pelaez, Phys. Rev. D 47 (1993) 4883; Phys. Rev. D 56 (1997) 3057; J.A. Oller, E. Oset and J.R. Pelaez, Phys. Rev. Lett. 80 (1998) 3452; Phys. Rev. D 59 (1999) 0740001; 60 (1999)

099906(E); F. Guerrero and J.A. Oller, Nucl. Phys. B 537 (1999) 459; A. Dobado and J.R. Pelaez, Phys. Rev D 65 (2002) 077502; A. Filipuzzi, J. Portoles and P. Ruiz-Femenia, JHEP 1208, 080 (2012); PoS CD 12, 053 (2013).

[21] V. Gribov ; *Strong Interactions of Hadrons at high Energies*. Cambridge University Press (2009).

[22] J.M. Cornwall, D.N. Levin and G.Tiktopoulos, Phys. Rev. D10 (1974) 1145; C. E. Vayonakis, Lett. Nuovo Cim. 17, 383 (1976).; B.W. Lee, C. Quigg and H. B. Thacker, Phys. Rev. D16 (1977) 1519; G.J. Gounaris, R. Kogerler and H. Neufeld, Phys. Rev. D34 (1986) 3257; M.S. Chanowitz and M.K. Gaillard, Nucl. Phys. B261 (1985) 379; A. Dobado and J.R. Pelaez, Nucl.Phys. B425 (1994) 110; Phys. Lett. B329 (1994) 469; C. Grosse-Knetter and I.Kuss, Z.Phys. C66 (1995) 95; H.J.He,Y.P.Kuang and X.Li, Phys. Lett. B329 (1994) 278.

[23] D. Espriu and J. Matias, Phys. Rev. D 52 (1995) 6530.

[24] A. Dobado, et al. *Effective Lagrangians for the Standard Model*. Springer, Berlin (1997).

[25] R. Delgado, A. Dobado and F. Llanes-Estrada, JHEP 1402, 121 (2014);

[26] P. Arnan, D. Espriu (Advisor), `http://hdl.handle.net/2445/59727`

[27] G. L. Kane, W. W. Repko and W. B. Rolnick, Phys. Lett. B 148, 367 (1984); S. Dawson, Phys. B 249, 42 (1985); M. S. Chanowitz and M. K. Gaillard, Nucl. Phys. B 261, 379 (1985).

[28] G. Barton, *Introduction to Advanced Field Theory*. John Wiley & Sons, London (1963).

[29] M. Low, A. Tesi and L. T. Wang, arXiv:1507.07557; D. Kim, K. Kong, H. M. Lee and S. C. Park, arXiv:1507.06312; L. Bian, D. Liu and J. Shu, L. A. Anchordoqui, I. Antoniadis, H. Goldberg, X. Huang, D. Lust and T. R. Taylor, arXiv:1507.05299; W. Chao, arXiv:1507.05310; Y. Omura, K. Tobe and K. Tsumura, arXiv:1507.05028; M. E. Krauss and W. Porod, arXiv:1507.04349; C. H. Chen and T. Nomura, arXiv:1507.04431; V. Sanz, arXiv:1507.03553; G. Cacciapaglia, A. Deandrea and M. Hashimoto, arXiv:1507.03098; C. W. Chiang, H. Fukuda, K. Harigaya, M. Ibe and T. T. Yanagida, arXiv:1507.02483; B. A. Dobrescu and Z. Liu, arXiv:1507.01923; A. Carmona, A. Delgado, M. Quiros and J. Santiago, arXiv:1507.01914; T. Abe, T. Kitahara and M. M. Nojiri, arXiv:1507.01681; T. Abe, R. Nagai, S. Okawa and M. Tanabashi, G. Cacciapaglia and M. T. Frandsen, arXiv:1507.00900; Q. H. Cao, B. Yan and D. M. Zhang, arXiv:1507.00268; J. Brehmer, J. Hewett, J. Kopp, T. Rizzo and J. Tattersall, arXiv:1507.00013; A. Thamm, R. Torre and A. Wulzer, arXiv:1506.08688.